Proceedings of the ASME 2016 International Design Engineering Technical Conferences and Computers and Information in Engineering Conference
IDETC/CIE 2016
August 21-24, 2016, Charlotte, North Carolina

DETC2016-60431

SAMPLE-BASED DESIGN OF FUNCTIONALLY GRADED MATERIAL STRUCTURES

Xingchen Liu
Spatial Automation Laboratory
University of Wisconsin - Madison
Madison, Wisconsin 53706
Email: xingchen@wisc.edu

Vadim Shapiro
Spatial Automation Laboratory
University of Wisconsin - Madison
Madison, Wisconsin 53706
Email: vshapiro@wisc.edu

ABSTRACT

Spatial variation of material structures is a principal mechanism for creating and controlling spatially varying material properties in nature and engineering. While the spatially varying homogenized properties can be represented by scalar and vector fields on the macroscopic scale, explicit microscopic structures of constituent phases are required to facilitate the visualization, analysis and manufacturing of functionally graded material (FGM). The challenge of FGM structure modeling lies in the integration of these two scales. We propose to represent and control material properties of FGM at macroscale using the notion of material descriptors which include common geometric, statistical, and topological measures, such as volume fraction, correlation functions and Minkowski functionals. At microscale, the material structures are modeled as Markov random fields: we formulate the problem of design and (re)construction of FGM structure as a process of selecting neighborhoods from a reference FGM, based on target material descriptors fields. The effectiveness of the proposed method in generating a spatially varying structure of FGM with target properties is demonstrated by two examples: design of a graded bone structure and generating functionally graded lattice structures with target volume fraction fields.

1 Modeling of functionally graded material structures

1.1 Functionally graded materials

Functionally graded materials (FGMs) are heterogeneous materials made of two or more constituent phases with properties changing gradually with position [1]. The spatial variation (gradation) of properties is determined by changes in the geometric configuration of the constituent phases (a.k.a. *material structure*) that serve particular mechanical (or more generally, physical) function. FGMs are ubiquitous in nature due to their abilities to satisfy multifold functional constraints and adapt to conflicting requirements; this also explains why FGMs are a popular candidate as engineering materials. FGMs may be found in a broad spectrum of applications, including filters [2], wear resistant coatings [3], bone and dental implants [4,5,6], and cutting tools [7, 8]. Teeth [4], bones [5] and bamboos [9, 10] are a few examples of FGM in nature.

Traditionally, the modeling of FGM focuses on the level of macroscopic properties [11, 12, 7]. However, it is the underlying spatial variation of material structures that create and control the spatially varying properties. Recent advances in additive manufacturing [1, 13, 14, 15] and exponentially growing computing power enables the shift of engineering design from the classical material selection paradigm into a simultaneous design of material composition and structure [16, 17]. Systematic modeling and design of graded structures with desired mechanical properties is a key ingredient of this paradigm shift. In this paper, we study the synthesis of two-phase structures, such as porous structures, from a reference material sample. The material structures are discretized into sets of voxels, which is consistent with the popular image acquiring techniques such as micro – computed tomography (μCT) and Magnetic resonance imaging (MRI).

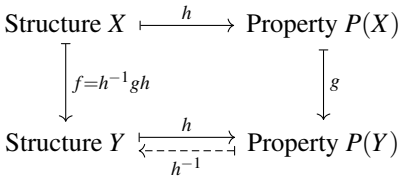

FIGURE 1: Key problem: construct a material structure Y with target effective material properties distribution $P(Y)$, given a material structure X with effective properties distributions $P(X)$. X and Y are usually represented by some microscopic models. Map h evaluates the effective properties of X and Y. Map g represents gradation techniques to design the target properties fields on macroscopic scale. Map f symbolizes the integration of macroscopic and microscopic representations.

1.2 Construction problems in material structure modeling

The basic construction problem of material structure modeling is illustrated in a commutative diagram as shown in Figure 1. We are typically given a reference material structure sample $X \subset R^3$ whose effective material properties $P(X)$ can be evaluated via map h: one of many known homogenization methods. For example, effective Young's modulus can be homogenized through various homogenization theories, including the Gibson model for cellular materials [18], Voigt - Ruess bounds, Hashin - Strikman bounds [19], Green's function based method [20,21], and power law [22] which is frequently used in SIMP-based topology optimization [23]. Note that $P(X)$ may be evaluated at any point of $p \in R^3$ whether it belongs to X or not, because homogenization h typically requires integrating and averaging of the mechanical properties in some neighborhood of p. We will denote the property evaluated at a point p as $P(p)$ when there is no ambiguity.

The target properties fields $P(Y)$ can be designed by various gradation techniques (map g), such as interpolation schemes in solid modeling [7] and Solid Isotropic Material with Penalization (SIMP) [23] in topology optimization. Given the target macroscopic properties distribution, the result structure Y can either be calculated from X by updating the parameters of the microscopic model or from $P(Y)$ directly through inverse homogenization [24]. It appears that the solutions to both construction problems require knowledge of the inverse homogenization map h^{-1}. Unfortunately, the relationship between the effective material properties and the corresponding material structures that produce them are known only for some periodic and cellular structures but not in general [25]. When such relationship is not known, an iterative approach is often adopted: the structure Y is repeatedly updated and the properties $h(Y)$ evaluated until they match the target $P(Y)$. There are at least two problems with this approach. The homogenization procedure itself is a computationally expensive process that may require additional material samples and is difficult to automate. Furthermore, while the inverse homogenization approach completely disregards the input structure X, the microscopic model requires a complete understanding and parameterization of the generative process for the desired class of material structures which is not readily available for many natural and synthetic materials.

Recently, Liu and Shapiro [26] showed that Markov Random Field (MRF) texture synthesis techniques may be used to reconstruct stationary material structures. We recognize that MRF models material structures as a collection of neighborhoods and texture synthesis rearranges neighborhoods so that both the microscopic geometry and macroscopic statistics are preserved (the macroscopic statistics are constant fields in case of stationary material structures). In the Jordan curve example, we observe that the microscopic geometry is preserved even though the macroscopic information is lost when the material structure is not stationary. This inspires us to devise a mechanism to guide the synthesis process by a target field, which controls macroscopic properties distribution while preserving the microscopic geometry of the material structure.

1.3 Contributions and outline

After reviewing the related macroscopic properties models and microscopic material structure models in Section 2, we propose the sample - based FGM structure design framework with its three pillars: construction by neighborhood, effective properties via descriptors, and texture synthesis to rearrange neighborhoods in Section 3. A given material sample X is modeled as a Markov Random Field (MRF), which assumes the joint probabilities of material distribution are local and views X as a collection of neighborhoods (Section 3.1). To circumvent the expensive numerical evaluation of neighborhood effective properties, we propose to represent and control material properties $P(Y)$ of FGM in terms of material descriptors, a collection of geometric and topological measures that correlate closely with many effective material properties (Section 3.2). The problem of design an FGM structure Y is formulated as a process of selecting neighborhoods in X according to the target descriptors fields. To solve the problem computationally, material structures are discretized on a regular lattice. Building on ideas from texture synthesis, the FGM structure design problems are solved by combining the influence of material descriptor fields and adjoining neighborhoods (Section 3.3). When it is possible, the proposed framework generates spatially varying structures with target material descriptors with given neighborhood size. But not all target properties $P(Y)$ fields can be obtained using neighborhoods from a given sample X; hence we discuss the compatibility between the reference material X and target properties field $P(Y)$, which is closely related to the quality of synthesized structure Y (Section 3.4). The effectiveness of the proposed method is demonstrated by two ex-

amples: design of a graded bone structure and generating a functionally graded lattice structure with target volume fraction field (Section 4). Section 5 concludes with a discussion on possible ways to speed up the implementation.

2 Related research

2.1 Macroscopic FGM property modeling

Modeling of FGM properties has been a major research issue in solid modeling. Such properties are usually represented by a collection of scalar or vector fields defined over a geometric domain. Without trying to be exhaustive, the following is a small sample of work in this area. Park et al. [11] use a volumetric multi-texturing method representing a three-dimensional density gradient. Siu and Tan [12] model both the distribution and the orientations of composite laminates through a source based scheme. Biswas et al. [7] formulate the material function as an interpolation of properties associated with given material features by inverse distance weighting. Other representations of material function are largely consistent with different ways to represent solids, including explicit functions [27, 28], implicit representations [29] and spline tensor products [30, 28], to cite a few. Readers may refer [31] for a survey.

As an alternative, topology optimization allows to optimize some material property functions for thermal stress [32], displacement [33] and structural weight [34]. A discrete FGM may be designed for a structure by segmenting the density field generated in topology optimization [35]. Some of these researches realize material structures from designed properties by assuming a linear relation [31] or a power law [22] between material properties and volume fractions. However, a blend of constituent phases by their volume fractions cannot accurately represent the required spatially varying properties, as it does not carry geometry or topology information about the microstructure [36,37,38]. Even though these methods are unable to produce the material structure, they are useful in modeling and design of the target descriptor and property fields used in this paper.

2.2 Material structure modeling

Existing approaches on material structure modeling can be roughly divided into two categories: procedural methods and reconstructive methods. In procedural modeling, material structure is produced by an algorithmic process. For example, Laguerre tessellations are used for ceramic and aluminum foams modeling [39]; FRep models both regular lattice and irregular porous material through optimizing in the parameters space of a pseudo-random model [40]; a texture mapping system is designed to add internal structures into solids from a library [41]. Kou and Tan [42] use random Voronoi tessellation, with grains bounded by B-Splines to design irregular porous structure with controllable pore shapes. Kou and Tan's work is extended by grading the random distribution of Voronoi sites to model graded porous structure [43]. Procedural methods are effective geometric modeling tools, but they suffer from two major limitations: (1) procedural methods require a complete understanding and parameterization of the generative processes, which are unknown for vast majority of natural and synthetic physical processes; (2) direct relationship between procedural models and their effective bulk material properties is known only in a few special cases, and cannot be established in general. These disadvantages make procedural methods limit their applications in the design of FGM structures.

Reconstructive methods seek to generate material structures directly from given descriptors and/or bulk material properties that are estimated from given reference material samples. The most common approach is to focus on matching material descriptors, especially two-point correlation functions, between a given reference sample and the desired reconstruction result by solving a large-scale stochastic optimization problem [44, 45]. One advantage of the optimization-based approach is its applicability to a broad range of random heterogeneous materials because it does not depend on the stochastic process by which a material structure is formed [37]. When the reference structure is abstracted by its descriptors, important structural (geometric and topological) details of the reference material are usually lost. This implies that optimization-based approaches will reconstruct similar material structures for distinct reference materials with similar descriptors. Efforts to address this accuracy issue include using higher order correlation functions [46], including two-point cluster function into the target function of the optimization as a hybrid method [47], and implementing a dilation-erosion scheme [48]. However, once the geometric and topological information about the structure is lost, it cannot be fully recovered.

Another related problem is inverse homogenization, in which a material structure is constructed to satisfy prescribed positive semi-definite constitutive tensors [24]. This problem appears to be solved only for a few periodic structures using unit cells. An FGM may be constructed by designing each unit cell individually [49], which is computationally very expensive and impractical for real applications. Designing unit cells with different effective constitutive properties is not the topic of present study.

Texture synthesis techniques have recently been used for material reconstruction by several researchers [50,51,26,52]. In particular, Liu and Shapiro [26] demonstrated that Markov random field texture synthesis can be used to reconstruct a variety of periodic and random heterogeneous structures while preserving their geometric, topological, and physical properties. The classical texture synthesis can reconstruct only stationary material structures that remain (statistically) invariant under translation [53, 54]. Such structures cannot be graded in a controlled fashion. Later advances in the field [55, 56, 57] use an external control field to influence and to guide placement of next pixel

(patch or material element). This relaxes the requirement of global stationarity in texture synthesis process and makes it controllable.

3 Problem Formulation

3.1 Construction by neighborhoods

We model the reference material structure X and the target structure Y as Markov random fields (MRFs). MRF assumes probabilities of material distribution are local, i.e. the material structure at any point depends on only the neighboring points. A refined version of the commutative diagram in Figure 1 is shown in Figure 2. It acknowledges explicitly that the reference material structure X and the target structure Y are collections of neighborhoods $N(X)$ and $N(Y)$ respectively. All neighborhoods are assumed to be of size s, selected to be large enough to give a meaningful description of the microscopic material structure.

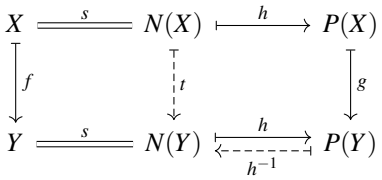

FIGURE 2: Design and reconstruction of graded material structures are reformulated in terms of neighborhoods.

We can now restate the generic material structure construction problem more concretely in terms of neighborhoods: given a material structure X with effective properties $P(X)$, construct material structure Y, such that:

$$\exists x \in X \quad s.t. \quad N(y) = N(x) \quad \text{and} \quad h(N(y)) = P(y), \quad \forall y \in Y \tag{1}$$

The two conditions are related but are not redundant. The matching of the neighborhoods simply reflects the requirement that the geometry and composition of the material structure Y originates from the reference structure X. The second condition acknowledges that the similarity of neighborhoods may not be sufficient to guarantee the desired target properties $P(Y)$. The conditions are not always independent, because neighborhoods with similar geometric and topological properties may indeed possess similar effective material properties, and it is conceivable that neighborhoods with many matching effective properties may indeed be very similar geometric properties.

In all cases, the material structure construction problem has been reduced to the problem of matching and selecting neighborhoods in the reference structure X and reassembling them in the target structure Y by a map t shown as a dashed arrow in Figure 2. This map will be discretized and implemented using texture synthesis techniques in Section 3.3. We also observe that the reformulation in terms of neighborhoods reduced the difficult inverse homogenization problem to a problem of filtering: only those neighborhoods in $N(X)$ that have desired material properties $g(P(X))$ will be selected for use in the target material structure $N(Y)$.

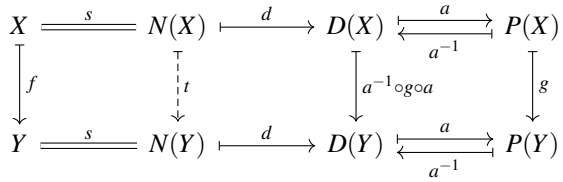

FIGURE 3: Problem formulation via material descriptors.

3.2 Effective material properties via descriptors

Another obstacle to solving the FGM structure design problem is the need to evaluate material property P on any neighborhood in the reference materials. This is a non-trivial task that usually involves solving multiple boundary value problems [58], making the reconstruction procedure inefficient and impractical.

Instead, we propose to replace material properties $P(X)$ by their proxies: a collection of geometric, topological, and statistical material descriptors $D(X)$ that are easily computable for a given neighborhood $N(x)$ of the material structure. Specific examples of $D(X)$ include correlation functions [37] and Minkowski functionals [59]. Numerous studies focus on relating the effective material properties with material descriptors because the latter can be measured directly. Examples include volume fraction and Voigt-Reuss bound [60], n-point correlation functions and elastic properties [61], Minkowski functionals and osteoporosis [62], and total number of aggregates and performance of tires [63].

Using material descriptors allows us to transform the commutative diagram in Figure 2 into the one shown in Figure 3. The map a represents the relationship between material properties $P(X)$ and their material descriptors $D(X)$. Just like material properties, material descriptors $D(X)$ are spatially varying fields that are computed on fixed size neighborhoods in X and can be evaluated at any point $x \in R^3$ yielding $D(x)$. When map a is invertible, there is a one-to-one correspondence between properties $P(X)$ and descriptors $D(X)$. With this assumption, selecting neighborhoods $N(Y)$ possessing properties $P(Y)$ becomes equivalent to matching material descriptors $D(Y)$. The latter task is much simpler because it involves only geometric computations. It is noted that numerical homogenization such as Finite Element Method can still be used for properties that do not have an associated homogenization theory or whenever is deemed reasonable.

3.3 Neighborhood rearrangement via texture synthesis

To solve the proposed problem computationally, we discretize the material structures on an orthogonal lattice grid. The neighborhood of a point $x \in R^3$ is approximated by an orthogonal (rectangular in 2D) lattice neighborhood centered at x (Figure 4):

$$N(x) = \{y : \|y - x\|_\infty \leq \frac{s}{2}\} \tag{2}$$

where s is the given neighborhood size. The design objective (Equation 1) can be solved by relaxing into an optimization problem: searching for Y such as the energy

$$E = \int_Y [\alpha \min_{x \in X}(\|N(x) - N(y)\|) + (1-\alpha)(\|d(N(y)) - D(y)\|)]dy \tag{3}$$

is minimized. Note that we use $D(y)$ and map d as the surrogates for $P(y)$ and map h as discussed in the previous section. $\min_{x \in X}(\|N(x) - N(y)\|)$ finds the best matching neighborhood in $N(X)$ and $\|d(N(y)) - D(y)\|$ measures the difference between the actual descriptors of $N(y)$ and target descriptors $D(y)$.

The optimization problem (Equation 3) is $NP-hard$ [64] and all existing techniques compute approximations to the optimal solutions [53, 65, 66]. In the present study, the graph-cut texture synthesis algorithm [56, 64] is adopted:

1. Determine $N(Y)$ neighborhood by neighborhood in steps of $s - o$ in raster (lexicographic) order (Figure 4), where o is the size of overlap between adjacent neighborhoods.
2. For each neighborhood $N(y)$, the best matching neighborhood in X is selected from $N(X)$ based on the weighted combination:

$$d_{total} = \alpha d_N + (1-\alpha) d_D, \tag{4}$$

where d_N measures the difference between $N(y)$ and all neighborhoods in $N(X)$ within the overlap region:

$$d_N(x) = \sum_{(i,j) \in overlap} |N_i(x) - N_j(y)| \tag{5}$$

and d_D represents the weighted difference of all material descriptors between $D(X)$ and $D(y)$:

$$d_D(x) = \sum_{i=1,2...k} w_i |D_i(x) - D_i(y)| \tag{6}$$

3. Compute the voxel-wise mismatch over the overlap region (Figure 4). Use graph-cut algorithm [67] to find the optimal hypersurface (a curve in 2D and a surface in 3D) that separates the overlap region in two parts while minimizing the accumulated mismatches along the boundary.

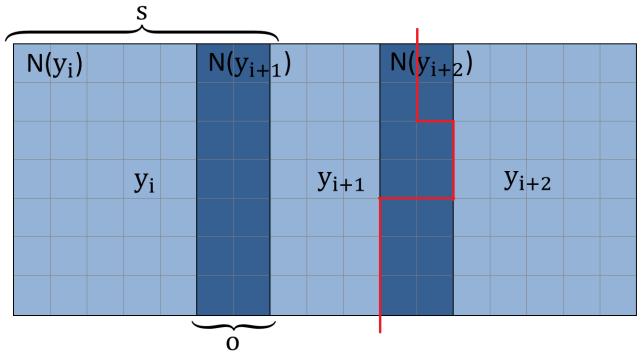

FIGURE 4: Synthesis of Y neighborhood by neighborhood in steps of $s - o$. For this illustration, $s = 7$ is the neighborhood size, $o = 2$ is the size of overlap. The red curve illustrates the hypersurface that separates the overlap region in two parts while minimizing the accumulated mismatches along the boundary.

The algorithm solves Equation (3) with the following three approximations: (1) rather than for all neighborhoods in Y, the neighborhoods and material descriptors constraints are checked in steps of $s - o$; (2) the total energy E is minimized in a "greedy" fashion: in raster order, the best fit is chosen for each neighborhood; (3) $d(N(y))$ in Equation 3 is approximated by $d(N(x))$, given the best matching $N(x)$ eventually becomes $N(y)$.

Even though the algorithm involves a significant amount of approximation, it is able to duplicate a stationary material structure with guaranteed accuracy by consistently estimating the joint distribution as well as material descriptors on a predefined neighborhood window [54, 26]. The practical implication of this result is two-fold: (1) any neighborhood $N(y)$ in the duplicated structure Y almost surely exists in its counterpart reference structure X, i.e. we expect that N(Y) $\subset$ N(X); (2) the probability distributions of such neighborhoods with regards to both structures are also the same, as a direct consequence of the stationarity assumption. In contrast, the quality of the constructed graded material depends on the compatibility between reference material and target fields, which is the subject of next section.

3.4 The quality of the design result

In a typical design problem, target fields $D(Y)$ may be created directly as a scalar or vector field via a map g that could be a combination of various gradation techniques. It is not reasonable to expect that every such property $D(Y)$ can be realized by selecting neighborhoods in $N(X)$. For example, the system of Equations 1 may become "over constrained" when a target

property does not exist in the reference material or there are no adjacent neighborhoods in the reference structure satisfying the properties of the adjacent neighborhood in the target field. As a result, the energy of Equation 3 can never decrease to 0. If there exists Y satisfying both conditions in Equation 1, we say that the target fields $D(Y)$ are *compatible* with given reference material X and neighborhood size s. When $D(Y)$ is compatible, the optimal solution of minimizing Equation (3) is the exact solution of Equation (1); when the $D(Y)$ is incompatible, the minimizer of Equation (3) yields an approximate solution based on the weight α.

The "binary" definition above is often too restrictive to be true except for a few special cases, such as reconstructing a stationary periodic structure or when target descriptor fields $D(Y)$ is exactly the same as $D(X)$ (see bone reconstruction example in Section 4.1). Nonetheless, it gives some theoretical backgrounds on what to expect for the quality of the synthesized result Y: in real design scenarios, a perfect solution usually does not exist due to the lack of compatibility between the inputs. To quantitatively assess the quality of the result Y, we introduce the notion of (N,D) - *compatible*, where N measures the maximum mismatch between neighborhoods (d_N) and D measures the maximum deviation from target descriptors (d_D). It is noted that the same notion may extend to quantify the degree of compatibility between X, s, and $D(Y)$ by the quality of the optimal solution of Equation 3. Design problems satisfying the original compatibility definition are (0,0) - compatible with this new notion.

4 Experiment results

4.1 Femur bone reconstruction

In this section, we demonstrate the effectiveness of the proposed approach for reconstruction of a 2D (image of) femur bone structure (Figure 5(a)). Minkowski functionals are the preferred material descriptors in that they are standard measurements for bone structure characterization [68]. There are exactly $d+1$ for a d-dimensional material structure: volume, surface area, average mean curvature, and Euler characteristic for $d=3$, and area, perimeter, and Euler characteristics for $d=2$. Regions of different properties in bone structures can be differentiated by Minkowski functionals.

For ease of comparisons, both d_N and d_D in Equation 4 are normalized into range $[0,1]$. Three Minkowski functionals are equally weighted and α is chosen as 0.9. Both the reference and reconstruction results are discretized on a lattice of 399 by 343 pixels, with a fixed size neighborhood of 25 by 25 pixels. Figure 5 (b)-(d) show the fields of Minkowski functionals $D(X)$ for the reference bone structure X: area, perimeter and Euler characteristic. Since this is a reconstruction problem, the target descriptors fields $D(Y)$ are identical to $D(X)$. The inputs are (0,0) - compatible because X itself is the (0,0) - compatible solution we seek. Figure 5 (e) and (f) are reconstructions with and without the control of Minkowski functionals fields. As expected, reconstructions with Minkowski functionals fields are noticeably better than reconstructions without it. We successfully recovered the X since we are only selecting the neighborhoods in Figure 5 (a) targeting its own Minkowski functionals fields. It took 3.4s for a relatively inefficient MATLAB implementation to reconstruct Figure 5 (f) on an Intel Core i7 3.4 GHz CPU.

TABLE 1: Maximum and mean difference of Minkowski functionals between designed structures and original bone structures over designed region. Minkowski functionals are rescaled to [0, 1].

	Area		Perimeter		Euler characteristic	
	max	mean	max	mean	max	mean
Figure 6 (e)	0.2342	0.0178	0.1958	0.0121	0.3878	0.0467
Figure 6 (f)	0.3562	0.0236	0.2167	0.0177	0.4286	0.052

4.2 Bone structure design

Bone structures are vulnerable: diseases, physical injuries, and corticosteroids are among various reasons leading to their degradation. In rare cases, the deteriorated region needs to be removed and a bone scaffold may be implanted to stimulate the bone to regenerate itself as well as to bear loads. An ideal design of scaffold should mimic the bone structure in terms of mechanical properties, porosity and should be bio-compatible, bio-active or bio-resorbable to enhance tissue growth [69, 70]. With the assumption that a more natural shape would be more stimulating to bone regeneration process, it is possible to design the scaffold as the complement of the synthesized bone structure.

Figure 6 (a) shows a femur bone with deteriorated region removed. To design the target Minkowski functionals fields, we use the inverse distance interpolation [7] of Minkowski functionals values on the existing bone structure. In other words, Minkowski properties at any point are represented as the weighted sum of the properties known at some locations (typically points or boundaries), where the weights are inversely proportional to the powers of distances to these locations:

$$D(y) = \begin{cases} \sum_{i=1}^{N} \frac{D(y_i)}{d(y,y_i)^p} / \sum_{i=1}^{N} \frac{1}{d(y,y_i)^p}, & \forall i, d(y,y_i) \neq 0 \\ D(y_i), & \exists i, d(y,y_i) = 0 \end{cases} \quad (7)$$

where d is the Euclidean distance between two points and each y_i represents the center of an existing neighborhood in Figure 6 (a). Figure 6 (b) - (d) show the interpolated target descriptors fields with the power of distance equals 4. For non-convex domains, interpolation with interior distances may be advantageous [71].

Figure 6 (e) and (f) are generated bone structures from the

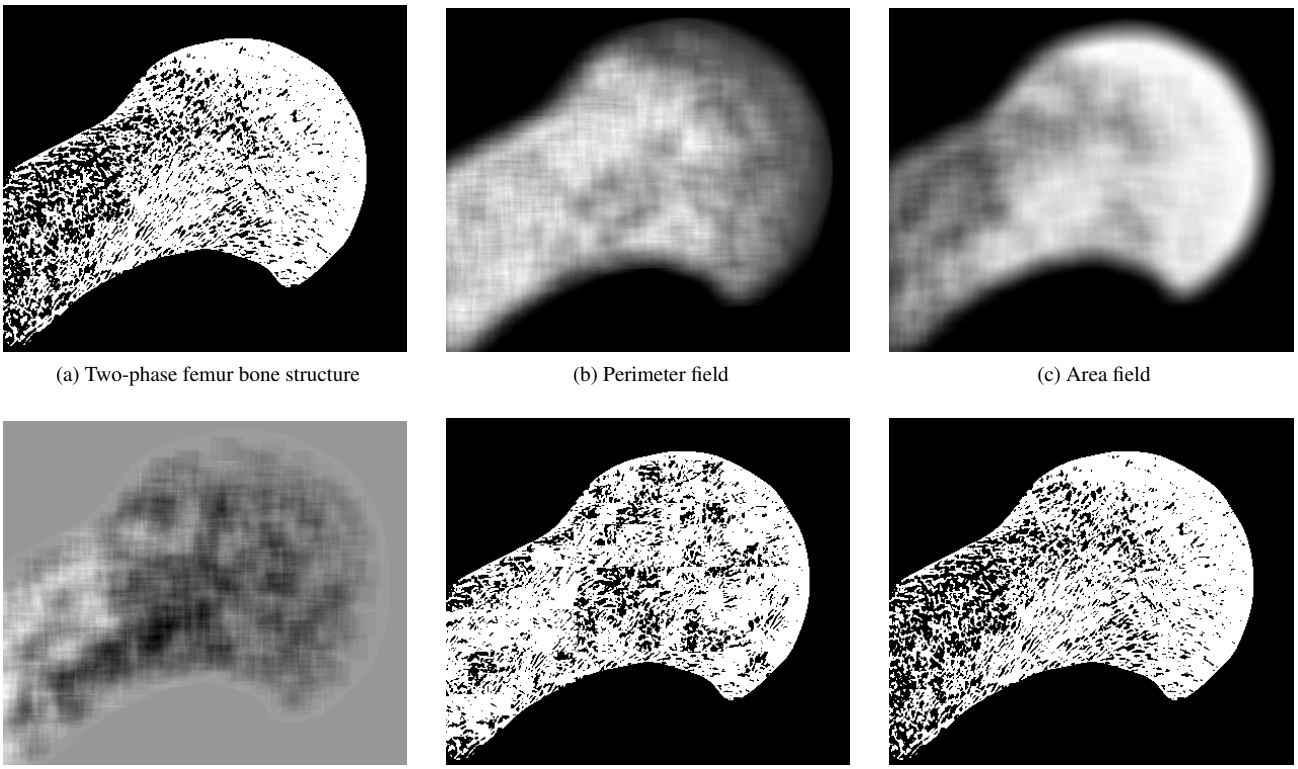

(a) Two-phase femur bone structure

(b) Perimeter field

(c) Area field

(d) Euler characteristic field

(e) Reconstruction without Minkowski functionals fields

(f) Reconstruction with Minkowski functionals fields

FIGURE 5: Femur bone structure reconstruction. (a) shows a cross-section of a two-phase femur bone structure, (b) - (d) are Minkowski functionals fields of (a), (e) and (f) are reconstruction results without and with Minkowski functionals as descriptors fields.

25 by 25 neighborhoods available in Figure 6 (a): with the target Minkowski functional fields calculated from the original intact bone (Figure 5 c) in (e), and with interpolated target Minkowski functional fields in (f). Note also that the proposed procedure connects the designed bone structures to the healthy part of (a) seamlessly. Mean and maximum differences between Minkowski functional values for the constructed results and those computed for the original bone sample in Figure 6 (a) are summarized in Table 1. The results suggest that using inverse-distance interpolated fields as target descriptor fields is a viable alternative to replacing the original descriptor fields (which are likely to be unknown). We expect that the construction results can be improved further when additional reference materials may be available for neighborhood selection, for example, additional healthy bone samples from other sources.

4.3 Functionally graded lattice structure

One obvious way to design the properties distributions of a functionally graded material is through optimization. We use Solid Isotropic Material with Penalization (SIMP), a popular method for topology optimization, to design the distribution of stiffness inside the design domain [72]. SIMP iteratively updates the volume fraction (relative density) distribution inside the design domain to optimize the design objective, such compliances, while meeting a set of constraints, such as a constraint on the total volume of the part. The power law is used as the homogenization model to establish the relationship between material descriptor (volume fraction) and material property (stiffness) while penalizing the intermediate densities. After the iteration

TABLE 2: Errors and compatibility of the 3D synthesis results.

	Volume fraction		Neighborhood	
	max	mean	max	mean
Figure 7 (d)	0.1004	0.0128	0.1450	0.0334
Figure 8 (b)	0.1700	0.0163	0.1253	0.0416
Figure 8 (d)	0.1378	0.0247	0.1327	0.0402
Figure 9 (d)	0.1481	0.0152	0.1791	0.0391

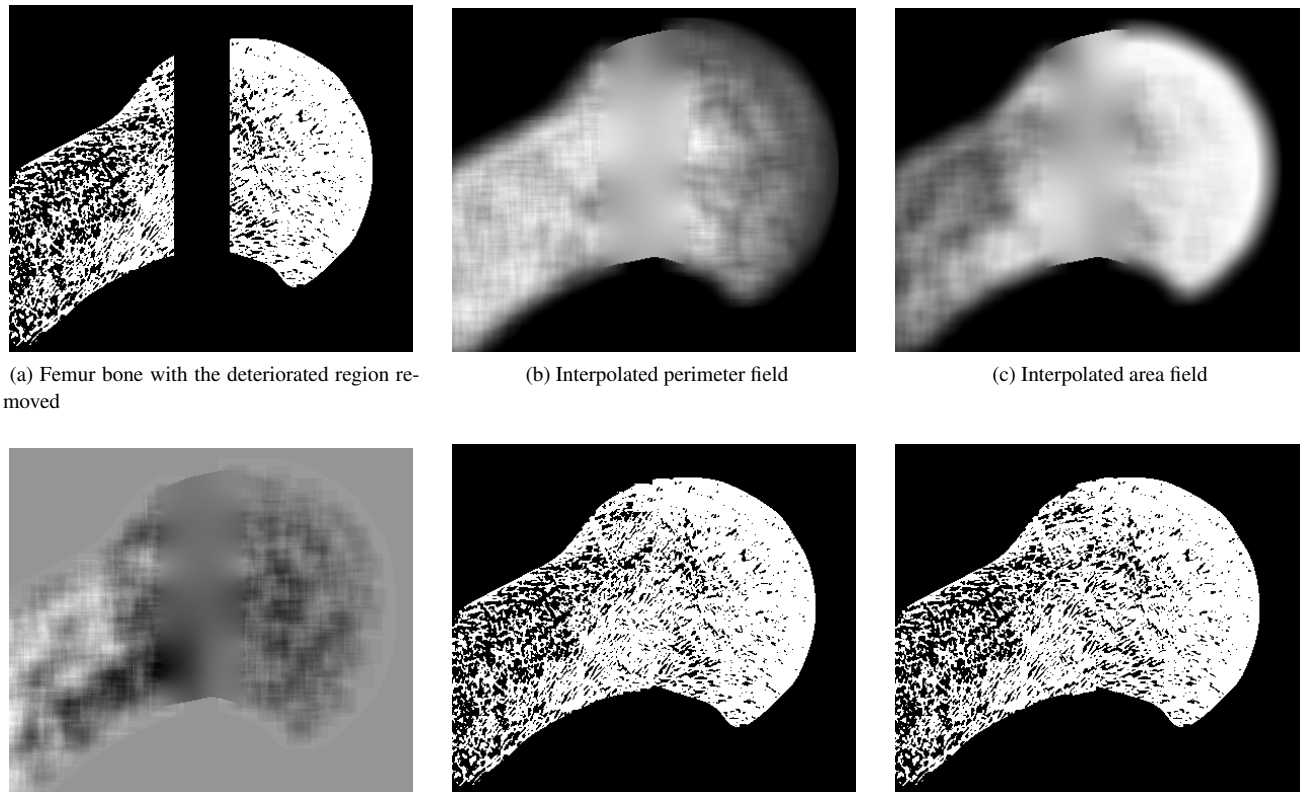

(a) Femur bone with the deteriorated region removed

(b) Interpolated perimeter field

(c) Interpolated area field

(d) Interpolated Euler characteristic field

(e) Design of missing bone structure with Minkowski functionals field from original bone sample (Figure 5(c)).

(f) Design of missing bone structure with Minkowski functionals field interpolated from existing structures.

FIGURE 6: Design of missing femur bone structures. (a) shows the Femur bone with missing bone structures. (b) - (d) are target Minkowski functionals fields designed by inverse distance interpolation from the healthy bone regions. (e) and (f) show the synthesized bone structures different target descriptors fields.

converges, the continuous volume fraction field is often thresholded to achieve a '0-1' design, but this is not necessary for our application. Instead, with the proposed method, we can fill the design space with any given material structures – random or periodic – according to the volume fraction field designed by SIMP. Here, we show that the proposed method performs equally well on periodic lattices.

Figure 7 demonstrates the design of a graded material structure that is functionally a cantilever beam with fixtures on the top and bottom left edges and downward loads on the bottom right edge. The target volume fraction distribution (Figure 7 a) is designed by SIMP with an overall volume fraction of 0.5. The lower and upper bounds of the volume fraction are 0.3 and 0.85. We set the penalty factor as one for a gradually varying volume fraction field. Figure 7 (c) shows the reference material: a procedurally generated spatially varying lattice. The synthesized structure is shown in Figure 7 (b) with a neighborhood size s of $14 \times 14 \times 14$ and 4 being the size of overlap along every direction. In some applications, such as 3D printing, the connectivity of the structure is very important: the generated structure is required to be a single connected piece. We enforce the connectivity by requiring every new neighborhood added to the synthesized structure to be a single connected one and connects to the existing neighborhoods. Other desirable properties such as smallest feature size can be guaranteed the same way by construction. It is noted that not all volume fractions in the target fields are realized in the reference lattice. As a result, some of the target volume fractions are achieved approximately. The compatibility of the result is summarized in Table 2. For comparison, Figure 7 (d) shows the graded lattice generated using the same procedural method as the reference structure.

We observe that the reference lattice can be constructed by two types of unit cells (Figure 8 a and c) that are dual to each other. The two types can be differentiated by their Euler characteristics χ: $\chi = 1$ for type 1 and $\chi = -4$ or 2 for type 2. The Euler characteristic of type 2 unit cell switches from -4 to

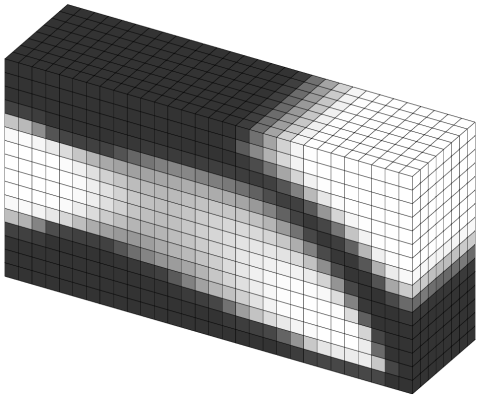

(a) Target volume fraction distribution from 0.3 to 0.85, $30 \times 16 \times 8$.

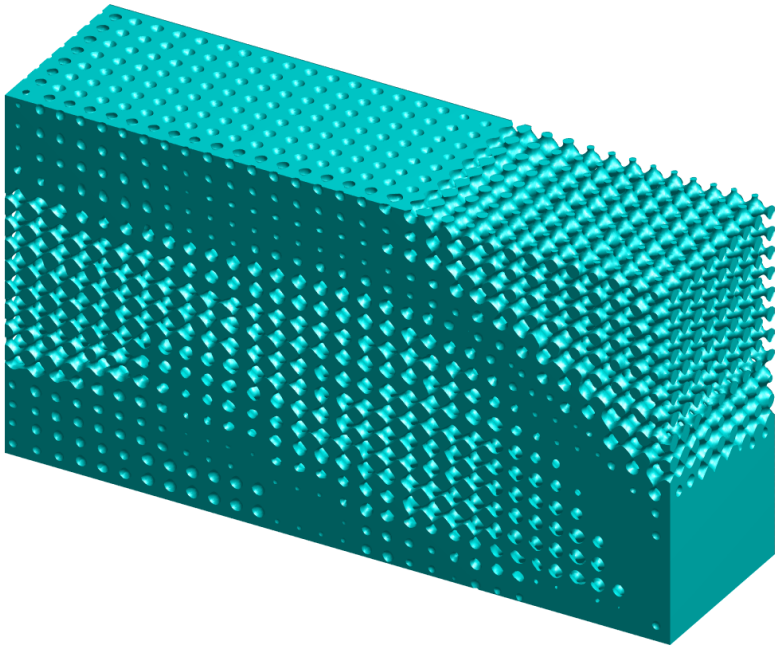

(b) FGM structure synthesized by the proposed framework, $300 \times 160 \times 80$.

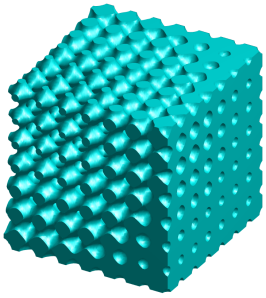

(c) Reference material, $80 \times 80 \times 80$.

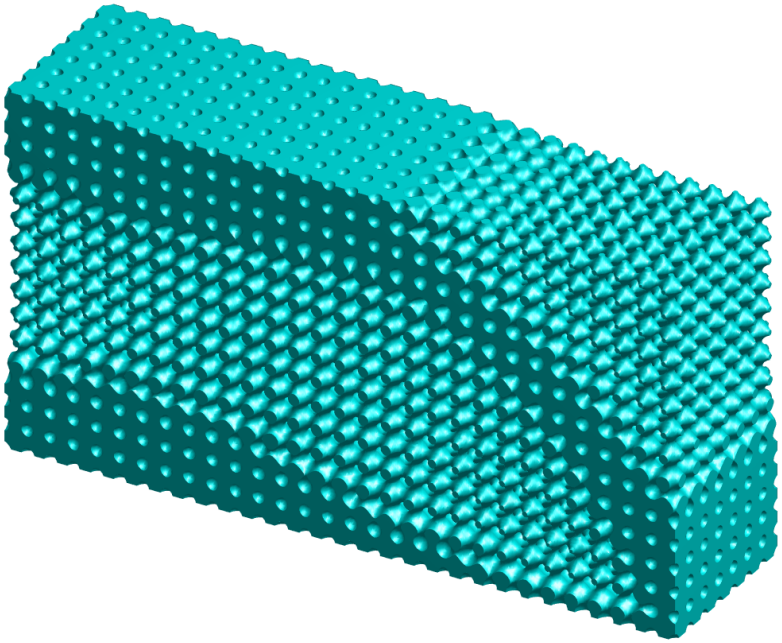

(d) FGM structure generated by procedural method, $300 \times 160 \times 80$.

FIGURE 7: Design of graded material structure that is functionally a cantilever beam with fixtures on the top and bottom left edges and downward loads on the bottom right edge. The target volume fraction field ranging from 0.3 to 0.85 is designed by SIMP with penalty factor equals 1.

2 with increasing volume fractions. $\chi = -4$ is calculated by gluing two triple torus ($\chi = -2$) together over a two-dimension circle ($\chi = 0$): $-4 = -2 \times 2 - 0$. With the Euler characteristics, we control the synthesis of the lattice structures by selecting neighborhoods of type 1 or type 2 unit cells only. The results are illustrated in Figure 8 (b) and (d), respectively.

Summarized in Table 2, the difference in neighborhoods is calculated as the ratio of the mismatched voxel to the volume of the overlap region. The errors of Figure 7 (d) are smaller than Figure 7 (b) and (d). This is because that in Figure 7 (d) the Euler characteristics are not constrained and there are more neighborhoods to choose from. Figure 9 shows an additional example of a wheel design with fixtures on four lower corners and load on the center of the bottom surface. The connectivity of the neighborhood is not enforced for this example and small disconnected pieces can be seen near the edges. The neighborhoods with disconnected pieces are hardly mistakes as they do exist in the reference material. The computation time of each example takes about 90 minutes, which is significantly longer than the two-dimensional cases. This is because the algorithm is linear in time to not only the number of neighborhoods to generate in Y, but also the number of neighborhoods to search for in X and the size of overlap and all of them are significantly larger in 3D. Possible acceleration schemes are discussed in Section 5.

5 Conclusion

We formulated the problems of design and reconstruction of functionally graded material structures as a process of selecting neighborhoods in a reference material sample. The new formulation allows to effectively bypass the difficult problem of inverse homogenization using techniques from Markov random field texture synthesis. We also introduced the notion of material descriptors, and Minkowski functionals in particular, to guide the construction of graded material structures, without the need to perform numeric homogenization or to solve boundary value problems. The fully implemented algorithm supports reconstruction and design of FGM structures by combining the influence of adjacent neighborhoods and target material descriptor fields in the neighborhood selection step of texture synthesis. We demonstrated the effectiveness of the proposed approach for reconstruction and design of graded bone structures as well as generating functionally graded lattice structures.

Many acceleration schemes have been proposed for 2D synthesis, including PatchMatch [65], Image melding [73], and PatchTable [66], whose core idea is to perform an approximate nearest neighborhood (ANN) search over $N(X)$. However, ANN search inevitably infects the quality of Y. In addition, most acceleration schemes work on two-dimension images and do not scale to three dimensions straightforwardly. To speed up without compromising the quality of the result, we may compute d_N only for those neighborhoods with small d_D. Obviously, searching for such a subset of $N(X)$ will not jeopardize the quality of Y if $D(Y)$ and X are (0,0) – compatible. However, if not fully compatible, eliminating too many candidate neighborhoods in $N(X)$ could result in more geometric discontinuities, which may in turn lead to undesirable physical defects (e.g. stress concentrations) in the designed structure Y. This is the main reason a weighted combination of d_N and d_D is adopted in Equation (3). To conclude, filtering $N(X)$ by $D(Y)$ should depend on the degree of compatibility and requires further studies.

An apparent limitation of the proposed method is that it cannot guarantee that the specified distribution of FGM properties is achieved, because this explicitly requires compatibility between the reference material structure and the target properties field. We note, however, that the notion of (N,D)-compatibility allows fine tuning the trade offs between the neighborhood and the descriptor incompatibilities. Methods for evaluating the compatibilities *a priori* appear to be a useful direction for future explorations. Remedies for large incompatibilities include modifyng the target properties field, enriching or modifying the reference material structure, or both. For example, the reference material structure may be modified using morphological operations to increase compatibility, but such modifications could also alter the properties of the reference material. New reference matertial structures could also be designed by other methods reviewed in Section 2, when the target properties are beyond the reach of the direct modification of the reference material structure.

ACKNOWLEDGMENT

This research was supported by NSF grants CMMI-1344205 and CMMI-1361862 and the National Institute of Standards and Technology. The responsibility for errors and omissions lies solely with the authors.

REFERENCES

[1] Birman, V., and Byrd, L. W., 2007. "Modeling and Analysis of Functionally Graded Materials and Structures". *Applied Mechanics Reviews,* ***60***(5), p. 195.

[2] Mahamood, R. M., Member, E. T. A., Shukla, M., and Pityana, S., 2012. "Functionally Graded Material : An Overview". *World Congress on Engineering,* ***III***, pp. 2–6.

[3] Ivar, E., 2004. "Functionally graded materials". In *K.W. James (Ed.), Handbook of advanced materials*. pp. 465–486.

[4] Zisis, T., Kordolemis, A., and Giannakopoulos, A. E., 2010. "Development of Strong Surfaces Using Functionally Graded Composites Inspired by Natural Teeth - Finite Element and Experimental Verification". *Journal of Engineering Materials and Technology,* ***132***(1), p. 011010.

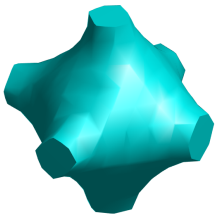

(a) Type 1 unit cell.

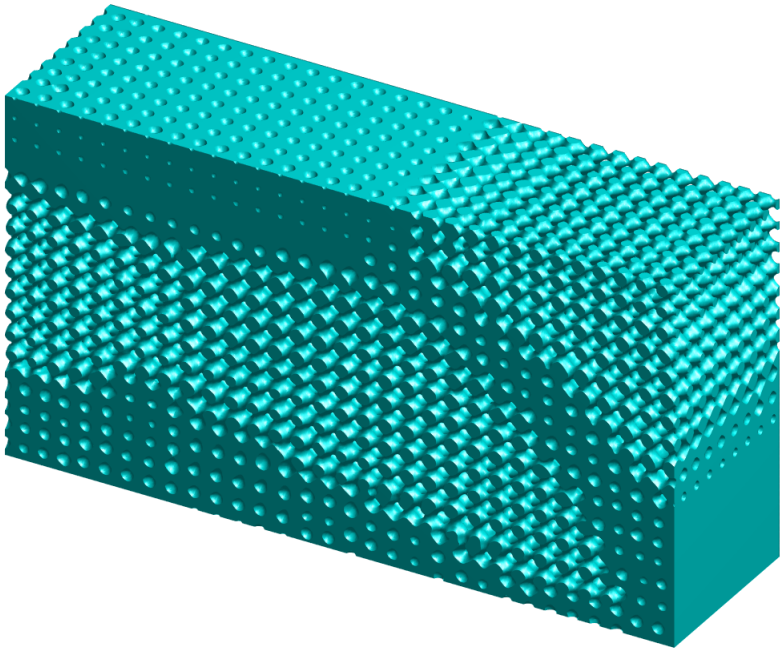

(b) FGM structure with type 1 unit cell.

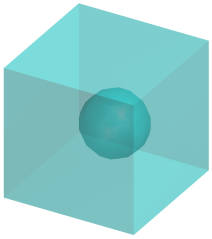

(c) Type 2 unit cell.

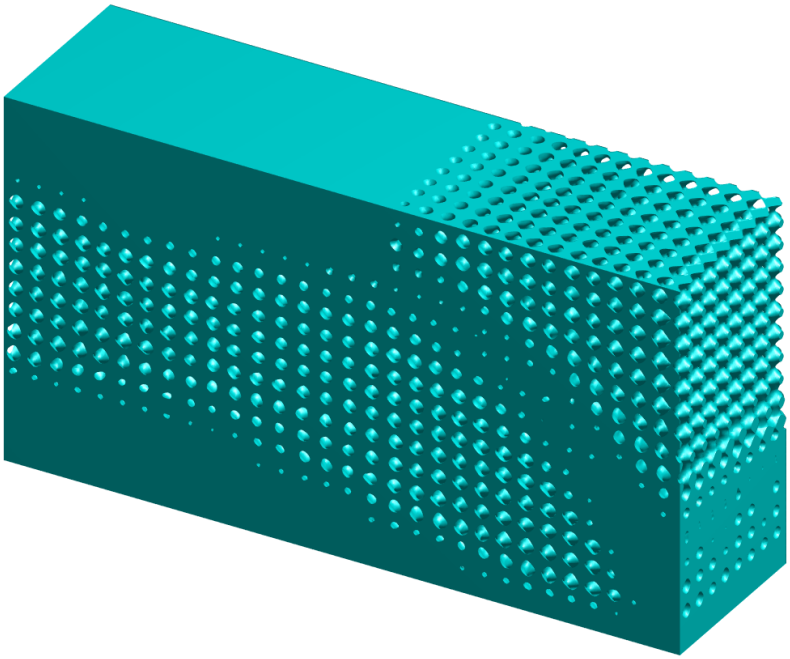

(d) FGM structure with type 2 unit cell.

FIGURE 8: Functionally graded lattice structures for a cantilever beam with different unit cells.

[5] Mehboob, H., and Chang, S.-H., 2015. "Optimal design of a functionally graded biodegradable composite bone plate by using the Taguchi method and finite element analysis". *Composite Structures,* ***119***, pp. 166–173.

[6] Thamaraiselvi, T. V., and Rajeswari, S., 2004. "Biological Evaluation of Bioceramic Materials - A Review". *Trends*

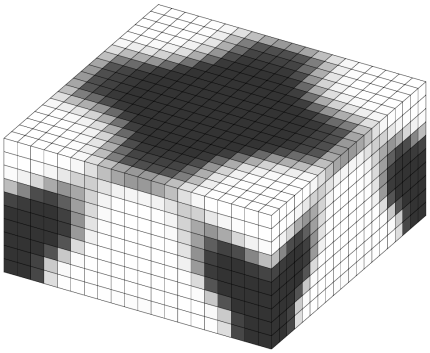

(a) Volume fraction distribution, $20 \times 20 \times 10$: view from top.

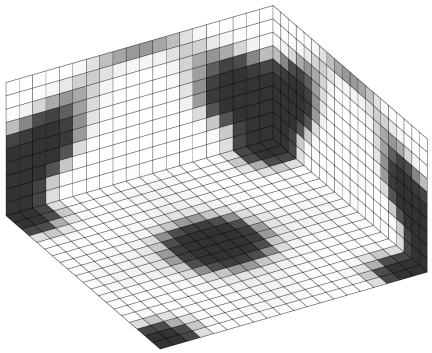

(b) Volume fraction distribution: view from bottom.

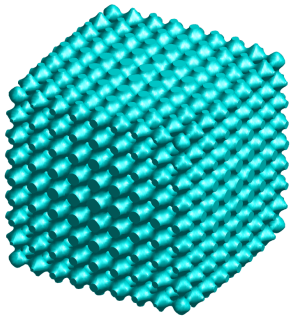

(c) Reference functionally graded lattice, $100 \times 100 \times 100$.

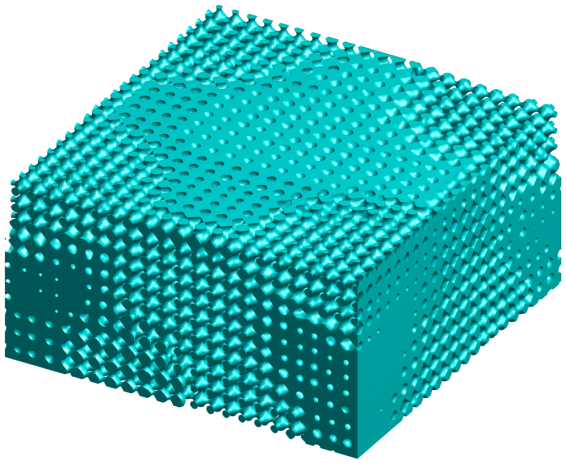

(d) FGM designed by the proposed framework: top. Resolution: $200 \times 200 \times 100$

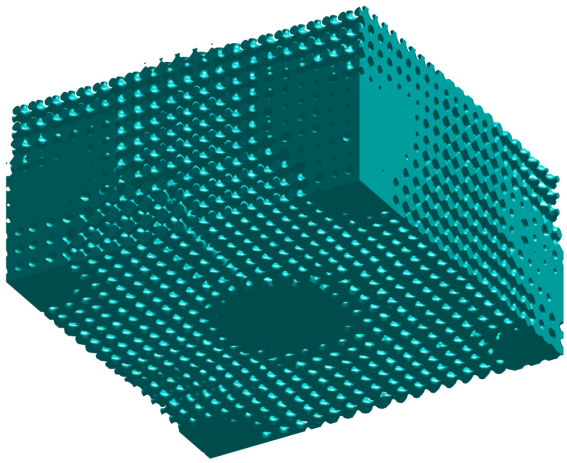

(e) Functionally graded structure designed by the proposed framework: bottom.

FIGURE 9: Design of graded material structure that is functionally a wheel structure with fixtures on four lower corners and load on the center of bottom surface. The target volume fraction field ranging from 0.3 to 0.85 is designed by SIMP with penalty factor equals 1.

Biomater. Artif. Organs, ***18***(1), pp. 9–17.

[7] Biswas, A., Shapiro, V., and Tsukanov, I., 2004. "Heterogeneous material modeling with distance fields". *Computer Aided Geometric Design,* ***21***(3), mar, pp. 215–242.

[8] Jaworska, L., Rozmus, M., Królicka, B., and Twardowska, A., 2006. "Functionally graded cermets". *Journal of Achievements in Materials and Manufacturing Engineering,* ***17***(1-2).

[9] Silva, E. C. N., Walters, M. C., and Paulino, G. H., 2006. "Modeling bamboo as a functionally graded material: Lessons for the analysis of affordable materials". *Journal of Materials Science,* ***41***(21), pp. 6991–7004.

[10] Nogata, F., and Takahashi, H., 1995. "Intelligent functionally graded material: Bamboo". *Composites Engineering,* ***5***(7), jan, pp. 743–751.

[11] Park, S.-M., Crawford, R. H., and Beaman, J. J., 2001. "Volumetric multi-texturing for functionally gradient material representation". In Proceedings of the sixth ACM symposium on Solid modeling and applications - SMA '01, SMA '01, ACM, pp. 216–224.

[12] Siu, Y. K., and Tan, S. T., 2002. "'Source-based' heterogeneous solid modeling". *CAD Computer Aided Design,* ***34***(1), jan, pp. 41–55.

[13] Oxman, N., Keating, S., and Tsai, E., 2011. "Functionally Graded Rapid Prototyping". In *Innovative Developments in Virtual and Physical Prototyping*. CRC Press, sep, pp. 483–489.

[14] Vidimče, K., Wang, S.-P., Ragan-Kelley, J., and Matusik, W., 2013. "OpenFab". *ACM Transactions on Graphics,* ***32***(4), p. 1.

[15] Doubrovski, E., Tsai, E., Dikovsky, D., Geraedts, J., Herr, H., and Oxman, N., 2014. "Voxel-based fabrication through

material property mapping: A design method for bitmap printing". *Computer-Aided Design*.

[16] Seepersad, C. C., Allen, J. K., McDowell, D. L., and Mistree, F., 2006. "Robust Design of Cellular Materials With Topological and Dimensional Imperfections". *Journal of Mechanical Design,* ***128***(6), p. 1285.

[17] Corney, J., and Torres-Sanchez, C., 2008. "Towards functionally graded cellular microstructures". *Journal of Mechanical Design,* ***131***(September 2009), pp. 1–7.

[18] Gibson, L. J., and Ashby, M. F., 1997. *Cellular solids: structure and properties*. Cambridge university press.

[19] Hashin, Z., and Shtrikman, S., 1963. "A variational approach to the theory of the elastic behaviour of multiphase materials". *Journal of the Mechanics and Physics of Solids,* ***11***(2), pp. 127–140.

[20] Moulinec, H., and Suquet, P., 1998. "A numerical method for computing the overall response of nonlinear composites with complex microstructure". *Computer Methods in Applied Mechanics and Engineering,* ***157***(1-2), pp. 69–94.

[21] Liu, X., and Shapiro, V., 2016. "Homogenization of material properties in additively manufactured structures". *Computer-Aided Design*, In Press, Accepted Manuscript.

[22] Bendsøe, M. P., and Sigmund, O., 1999. "Material interpolation schemes in topology optimization". *Archive of Applied Mechanics,* ***69***(9-10), pp. 635–654.

[23] Bendsøe, M. P., 1989. "Optimal shape design as a material distribution problem". *Structural Optimization,* ***1***(4), pp. 193–202.

[24] Sigmund, O., 1994. "Materials with prescribed constitutive parameters: An inverse homogenization problem". *International Journal of Solids and Structures,* ***31***(17), pp. 2313–2329.

[25] Gibson, L. J., and Ashby, M. F., 1982. "The Mechanics of Three-Dimensional Cellular Materials". *Proceedings of the Royal Society A: Mathematical, Physical and Engineering Sciences,* ***382***(1782), pp. 43–59.

[26] Liu, X., and Shapiro, V., 2014. "Random Heterogeneous Materials via Texture Synthesis". *Computational Materials Science,* ***99***, pp. 177–189.

[27] Liu, H., Maekawa, T., Patrikalakis, N. M., Sachs, E. M., and Cho, W., 2004. "Methods for feature-based design of heterogeneous solids". *CAD Computer Aided Design,* ***36***(12), pp. 1141–1159.

[28] Huang, J., Fadel, G. M., Blouin, V. Y., and Grujicic, M., 2002. "Bi-objective optimization design of functionally gradient materials". *Materials & Design,* ***23***(7), pp. 657–666.

[29] Pasko, A., Adzhiev, V., Schmitt, B., and Schlick, C., 2001. "Constructive hypervolume modeling". *Graphical models,* ***63***(6), pp. 413–442.

[30] Qian, X., and Dutta, D., 2003. "Design of heterogeneous turbine blade". *CAD Computer Aided Design,* ***35***(3), pp. 319–329.

[31] Kou, X., and Tan, S., 2007. "Heterogeneous object modeling: A review". *Computer-Aided Design,* ***39***(4), apr, pp. 284–301.

[32] Hu, Y., Blouin, V. Y., and Fadel, G. M., 2008. "Design for Manufacturing of 3D Heterogeneous Objects With Processing Time Consideration". *Journal of Mechanical Design,* ***130***(3), p. 031701.

[33] Cho, J. R., and Ha, D. Y., 2002. "Optimal tailoring of 2D volume-fraction distributions for heat-resisting functionally graded materials using FDM". *Computer Methods in Applied Mechanics and Engineering,* ***191***(29-30), pp. 3195–3211.

[34] Zhang, X. J., Chen, K. Z., and Feng, X. A., 2004. "Optimization of material properties needed for material design of components made of multi-heterogeneous materials". *Materials and Design,* ***25***(5), pp. 369–378.

[35] Wang, M. Y., and Wang, X., 2005. "A level-set based variational method for design and optimization of heterogeneous objects". *CAD Computer Aided Design,* ***37***(3), pp. 321–337.

[36] Panchal, J. H., Kalidindi, S. R., and McDowell, D. L., 2013. "Key computational modeling issues in Integrated Computational Materials Engineering". *Computer-Aided Design,* ***45***(1), jan, pp. 4–25.

[37] Torquato, S., 2002. *Random heterogeneous materials: microstructure and macroscopic properties*. Interdisciplinary applied mathematics: Mechanics and materials. Springer.

[38] Latief, F., Biswas, A., Fauzi, U., and Hilfer, R., 2010. "Continuum reconstruction of the pore scale microstructure for Fontainebleau sandstone". *Physica A: Statistical Mechanics and its Applications,* ***389***(8), apr, pp. 1607–1618.

[39] Redenbach, C., 2009. "Modelling foam structures using random tessellations". *Stereology and Image Analysis. Proc 10th Eur Congress of ISS,* ***4***.

[40] Pasko, A., Fryazinov, O., Vilbrandt, T., Fayolle, P.-A., and Adzhiev, V., 2011. "Procedural function-based modelling of volumetric microstructures". *Graphical Models,* ***73***(5), pp. 165–181.

[41] Chen, Y., 2007. "3D texture mapping for rapid manufacturing". *Computer-Aided Design and Applications,* ***4***(1-6), pp. 761–771.

[42] Kou, X., and Tan, S. S., 2010. "Modeling Functionally Graded Porous Structures with Stochastic Voronoi Diagram and B-Spline Representations". In 2010 International Conference on Manufacturing Automation, IEEE, pp. 99–106.

[43] Kou, X., and Tan, S., 2010. "A simple and effective geometric representation for irregular porous structure modeling". *Computer-Aided Design,* ***42***(10), oct, pp. 930–941.

[44] Yeong, C., and Torquato, S., 1998. "Reconstructing random media". *Physical Review E,* ***58***(1), jul, pp. 224–233.

[45] Jiao, Y., Stillinger, F., and Torquato, S., 2007. "Model-

ing heterogeneous materials via two-point correlation functions: Basic principles". *Physical Review E,* ***76***(3), sep, pp. 1–15.

[46] Graham-Brady, L., and Xu, X. F., 2008. "Stochastic Morphological Modeling of Random Multiphase Materials". *Journal of Applied Mechanics,* ***75***(6), p. 061001.

[47] Jiao, Y., Stillinger, F., and Torquato, S., 2009. "A superior descriptor of random textures and its predictive capacity". *Proceedings of the National Academy of Sciences*, pp. 1–6.

[48] Guo, E. Y., Chawla, N., Jing, T., Torquato, S., and Jiao, Y., 2014. "Accurate modeling and reconstruction of three-dimensional percolating filamentary microstructures from two-dimensional micrographs via dilation-erosion method". *Materials Characterization,* ***89***, mar, pp. 33–42.

[49] Zhou, S., and Li, Q., 2008. "Design of graded two-phase microstructures for tailored elasticity gradients". *Journal of Materials Science,* ***43***(15), pp. 5157–5167.

[50] Holdstein, Y., Fischer, A., Podshivalov, L., and Bar-Yoseph, P. Z., 2009. "Volumetric texture synthesis of bone micro-structure as a base for scaffold design". *2009 IEEE International Conference on Shape Modeling and Applications, SMI 2009*, jun, pp. 81–88.

[51] Sundararaghavan, V., 2014. "Reconstruction of three-dimensional anisotropic microstructures from two-dimensional micrographs imaged on orthogonal planes". *Integrating Materials and Manufacturing Innovation,* ***3***(1), jun, p. 19.

[52] Turner, D. M., and Kalidindi, S. R., 2016. "Statistical construction of 3-D microstructures from 2-D exemplars collected on oblique sections". *Acta Materialia,* ***102***, pp. 136–148.

[53] Wei, L.-Y., and Levoy, M., 2000. "Fast texture synthesis using tree-structured vector quantization". *Proceedings of the 27th annual conference on Computer graphics and interactive techniques - SIGGRAPH '00*, pp. 479–488.

[54] Levina, E., and Bickel, P. J., 2006. "Texture synthesis and nonparametric resampling of random fields". *The Annals of Statistics,* ***34***(4), aug, pp. 1751–1773.

[55] Ashikhmin, M., 2001. "Synthesizing natural textures". *Proceedings of the 2001 symposium on Interactive 3D graphics*, pp. 217–226.

[56] Efros, A. A., and Freeman, W. T., 2001. "Image Quilting for Texture Synthesis and Transfer". In Siggraph, Vol. 1, Los Angeles, California, USA, pp. 1–6.

[57] Zhang, J., Zhou, K., Velho, L., Guo, B., and Shum, H.-Y., 2003. "Synthesis of progressively-variant textures on arbitrary surfaces". *ACM Transactions on Graphics,* ***22***(3), p. 295.

[58] Zohdi, T. I., 2013. "Basic Microstructure-Macroproperty Calculations". In *Effective Properties of Heterogeneous Materials SE - 5*, M. Kachanov and I. Sevostianov, eds., Vol. 193 of *Solid Mechanics and Its Applications*. Springer Netherlands, pp. 365–389.

[59] Ohser, J., and Schladitz, K., 2009. *3D images of materials structures: processing and analysis*. Vch Pub.

[60] Hill, R., 2002. "The Elastic Behaviour of a Crystalline Aggregate". *Proceedings of the Physical Society. Section A,* ***65***(5), pp. 349–354.

[61] Kalidindi, S. R., Binci, M., Fullwood, D., and Adams, B. L., 2006. "Elastic properties closures using second-order homogenization theories: Case studies in composites of two isotropic constituents". *Acta Materialia,* ***54***(11), jun, pp. 3117–3126.

[62] Monetti, R., Bauer, J., Sidorenko, I., Müller, D., Rummeny, E., Matsuura, M., Eckstein, F., Lochmüller, E.-M., Zysset, P., and Räth, C., 2009. "Assessment of the human trabecular bone structure using Minkowski functionals". In Medical Imaging 2009: Biomedical Applications in Molecular, Structural, and Functional Imaging, X. P. Hu and A. V. Clough, eds., Vol. 7262, Society of Photo-Optical Instrumentation Engineers, p. 72620N.

[63] Xu, H., Dikin, D., Burkhart, C., and Chen, W., 2014. "Descriptor-based methodology for statistical characterization and 3D reconstruction of microstructural materials". *Computational Materials Science,* ***85***, apr, pp. 206–216.

[64] Kwatra, V., Schodl, A., Essa, I., and Turk, G., 2003. "Graphcut textures: Image and video synthesis using graph cuts". *ACM Transactions on*(2).

[65] Barnes, C., Shechtman, E., Finkelstein, A., and Goldman, D. B., 2009. "PatchMatch: A Randomized Correspondence Algorithm for Structural Image Editing". *ACM Transactions on Graphics,* ***28***(3), p. 1.

[66] Barnes, C., Zhang, F.-l., Lou, L., Wu, X., and Hu, S.-m., 2015. "PatchTable: Efficient Patch Queries for Large Datasets and Applications". *ACM Transactions on Graphics,* ***34***(4), pp. 97:1–97:10.

[67] Yuan, J., Bae, E., and Tai, X. C., 2010. "A study on continuous max-flow and min-cut approaches". *Proceedings of the IEEE Computer Society Conference on Computer Vision and Pattern Recognition*(1), pp. 2217–2224.

[68] Jiang, C., Giger, M. L., Chinander, M. R., Martell, J. M., Kwak, S., and Favus, M. J., 1999. "Characterization of bone quality using computer-extracted radiographic features.". *Medical physics,* ***26***(6), jun, pp. 872–9.

[69] Hutmacher, D. W., 2000. "Scaffolds in tissue engineering bone and cartilage.". *Biomaterials,* ***21***(24), pp. 2529–2543.

[70] Bose, S., Roy, M., and Bandyopadhyay, A., 2012. "Recent advances in bone tissue engineering scaffolds". *Trends in Biotechnology,* ***30***(10), pp. 546–554.

[71] Fryazinov, O., Sanchez, M., and Pasko, A., 2015. "Shape conforming volumetric interpolation with interior distances". *Computers & Graphics,* ***46***, pp. 149–155.

[72] Liu, K., and Tovar, A., 2014. "An efficient 3D topology optimization code written in Matlab". *Structural and Mul-*

tidisciplinary Optimization, pp. 1175–1196.

[73] Darabi, S., Shechtman, E., Barnes, C., Goldman, D. B., and Sen, P., 2012. "Image melding: combining inconsistent images using patch-based synthesis". *ACM Transactions on Graphics,* ***31***(4), pp. 1–10.